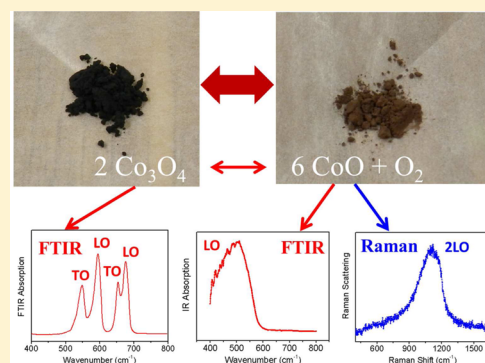


Identification of Cobalt Oxides with Raman Scattering and Fourier Transform Infrared Spectroscopy

Yang Li,[†] Wenlan Qiu,[‡] Fan Qin,[‡] Hui Fang,[§] Viktor G. Hadjiev,^{||} Dmitri Litvinov,^{†,‡} and Jiming Bao^{*,†,‡}[†]Department of Electrical and Computer Engineering and [‡]Materials Science and Engineering, University of Houston, Houston, Texas 77204, United States[§]Department of Physics, Sam Houston State University, Huntsville, Texas 77341, United States^{||}Texas Center for Superconductivity and Department of Mechanical Engineering, University of Houston, Houston, Texas 77204, United States

ABSTRACT: Although Raman spectral fingerprints of Co_3O_4 have been well established, the infrared spectrum of Co_3O_4 is less understood due to its dependence on sample morphologies and experimental configurations. The same is true for both Raman and infrared spectra of CoO . In this study, we present a comprehensive optical characterization of Co_3O_4 and CoO with Raman scattering and Fourier transform infrared spectroscopy (FTIR). Two of the transverse optical (TO) phonons and their corresponding longitudinal optical (LO) phonons of Co_3O_4 above 500 cm^{-1} are observed in both transmission and diffuse reflectance with LO/TO intensity ratios depending on particle size and the incident angle of FTIR beam. CoO is featured by a broad infrared band around 510 cm^{-1} . In contrast to many previous reports, no Raman-active phonon line is observed, which is in agreement with the selection rule for rock-salt CoO . Nevertheless, CoO can still be characterized by Raman scattering from magnetic excitations in its antiferromagnetic phase at low temperature and a two-phonon Raman band at $\sim 1060\text{ cm}^{-1}$.



1. INTRODUCTION

As the only two stable oxides of cobalt, Co_3O_4 and CoO have attracted increasing attention due to their remarkable magnetic, optical, electronic, and chemical properties. They have found a wide range of applications in catalysis, lithium-ion battery, solar energy, spintronics, and gas sensing.^{1–10} Nanostructures of cobalt oxides with different morphologies and sizes have been synthesized for better performances or new applications. Raman scattering and Fourier transform infrared spectroscopy (FTIR) are powerful and noninvasive characterization techniques used to identify and characterize cobalt oxides but many of reported spectra do not agree with each other. For example, Tang et al. observed two broad Raman bands at 455 and 675 cm^{-1} in CoO nanoparticles,¹¹ but Wang and Zhang showed two bands at 477 and 671 cm^{-1} in CoO nanowires;¹² Gallant et al. observed higher frequency bands and assigned them to A_{1g} and E_g modes of CoO .¹³ Very different sets of three Raman bands were reported by several groups^{14–16} and were further assigned to A_{1g} , E_g , and T_{2g} modes by Ravindra et al.¹⁶ Four Raman bands were also reported by Choi et al. in CoO powders and CoO electrode.¹⁷ In contrast, earlier work by Struzhkin et al. showed that CoO does not have any phonon Raman bands in the similar range but has a two-phonon Raman peak at 697 cm^{-1} .¹⁸

For FTIR of CoO , it was understood that the spectrum is characterized by a transverse optical (TO) phonon below 400 cm^{-1} and a higher frequency longitudinal optical (LO) phonon

but different values of LO has been reported by many groups. Tang et al. reported a broad absorption band at 507 cm^{-1} from transmission of CoO powder sample;¹¹ Barakat et al. observed a similar absorption band below 500 cm^{-1} in CoO nanofibers.¹⁹ Using reflectance and subsequent modeling of dielectric function of single crystal, Kant et al. obtained a LO of 562.1 cm^{-1} .²⁰ Higher-frequency bands in the range of 577 and 598 cm^{-1} were also reported by Lenglet et al. and Pfeil et al.^{21,22}

For Co_3O_4 , the “standard” Raman spectrum was already established by one of the authors.²³ Infrared spectrum of Co_3O_4 was also investigated by Shirai et al., who obtained all IR-active phonon modes from reflection spectra in combination with Kramers–Kronig transformation and oscillator fit.²⁴ Absorption-like spectra of both TO and LO phonons were reported by Lenglet et al., who measured reflectance spectrum of oxidized Co plate.²¹ Their approach was simple except that oxidized cobalt contained mixed Co_3O_4 and CoO phases, and the phonon frequencies depended on the thickness of oxidized film and angle of incident IR beam.²¹ Despite these earlier works, only two instead of four absorption bands above 500 cm^{-1} were observed and used as the IR signature of Co_3O_4 by many groups with frequency varying from one group to another.^{11,22,25–33}

Received: November 15, 2015**Revised:** January 28, 2016**Published:** February 3, 2016

These apparent discrepancies and lack of well-established spectra make it difficult to accurately identify cobalt oxides and understand their basic properties and will hinder their potential device applications. Using highly pure cobalt oxide thin films and powders, we first show the observation of all four LO/TO bands in both transmission and diffuse reflectance modes and then we explain how the experimental configuration and particle size will affect the relative intensity of LO versus TO. Having established the infrared spectrum of Co_3O_4 , we identify the LO of CoO by correlating IR spectrum with oxidation state of Co between CoO and Co_3O_4 . Using laser-induced oxidation, we disprove the 697 cm^{-1} line as a two-phonon Raman but confirm the broad 1060 cm^{-1} band as a two-phonon Raman by the observation of a small spectral shift with different laser lines. Such a complete set of Raman and FTIR spectra will provide a guideline for the future identification of cobalt oxides.

2. SAMPLE PREPARATION AND CHARACTERIZATION

Cobalt oxide thin films and powders were prepared for Raman and FTIR study because they are the most common forms of nanomaterials. One hundred nanometers thick Co_3O_4 films for FTIR were deposited on double side polished silicon wafers using an AJA ATC 2200 ultrahigh vacuum DC magnetron sputtering system with argon and oxygen flow rates of 35 and 5 sccm, respectively. High purity Co_3O_4 powders were purchased from Sigma-Aldrich with average sizes of $10\text{ }\mu\text{m}$ and 50 nm . Particles with less than 50 nm ($10\text{--}50\text{ nm}$) were obtained by ball milling $10\text{ }\mu\text{m}$ Co_3O_4 powders for 16 h in a SPEX Mixer/Mill (SamplePrep 8000M). CoO powders were converted from $10\text{ }\mu\text{m}$ Co_3O_4 powders via thermal decomposition.¹⁰ In some cases, such-obtained CoO powders were further annealed in H_2 environment at $200\text{ }^\circ\text{C}$ for 2 h to remove residue Co_3O_4 .³⁴ The transformation from CoO to Co_3O_4 powders was achieved by annealing CoO powders on a hot plate in air at various temperatures up to $800\text{ }^\circ\text{C}$. A Co foil was also heated in air at $800\text{ }^\circ\text{C}$ to form a surface Co_3O_4 layer and was then thermally decomposed to become CoO thin film.

FTIR was performed using a Thermo Nicolet iS50 spectrometer equipped with a DTGS detector at room temperature in the range of $4000\text{--}400\text{ cm}^{-1}$. To perform diffuse reflective FTIR (DRFTIR) measurement, KCl was mixed with cobalt oxide powders. Raman measurements were performed using a Horiba Triax550 and a T64000 spectrometers in a backscattering configuration.

3. RESULTS AND DISCUSSION

3.1. LO and TO Spectra of Co_3O_4 Film by FTIR Transmission. Infrared absorption through transmission measurement is the most straightforward experimental configuration of FTIR for thin film samples. However, conventional transmission with IR incidence normal to the film can only probe TO; previous observations of both LO and TO bands were achieved in reflection mode. An easy method to avoid this drawback of conventional transmission is to rotate the sample so that incident beam has a large angle from the normal of the film.³⁵ As shown in Figure 1a,b, only in oblique incidence the electrical field of infrared beam is able to couple to the polarization of LO phonons. As expected, the spectrum in Figure 1c is dominated by two TO modes with normal incidence but when the incident angle increases, the corresponding LO modes begin to appear and become stronger. Note that the incident beam is not polarized, only

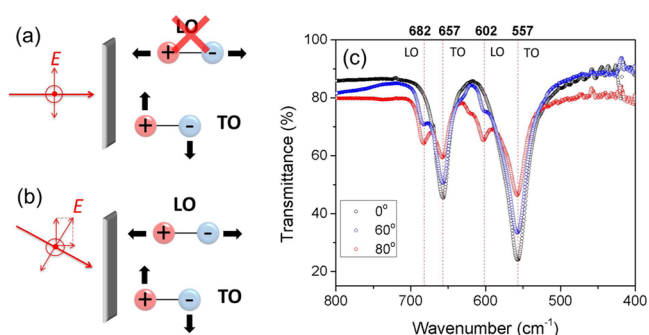


Figure 1. (a,b) Schematic for transmission measurement with (a) normal incidence and (b) oblique incidence. (c) FTIR transmission spectra of Co_3O_4 film on Si with three incident angles of 0° , 60° , and 80° .

p-polarized light is coupled to LO and s-polarized beam is not coupled to LO at any angles; this is why two TO bands are still stronger than LOs even at an angle of 80° . Another important observation is that the positions of all four phonons stay the same even when the angle varies.

3.2. LO and TO Spectra of Co_3O_4 Powders by Diffuse Reflectance FTIR. Transmission and reflection are good for thin films and thick single crystal samples with smooth surfaces, but for powder samples diffuse reflectance FTIR (DRFTIR) is a more convenient and effective method.¹⁰ Furthermore, DRFTIR allows people to obtain absorption spectrum through the Kubelka–Munk (KM) function $\text{KM}(R) = (1 - R)^2/2R \sim \alpha$, where R is diffuse reflectance and α is absorption coefficient. Figure 2 shows DRFTIR spectra of Co_3O_4 with three different

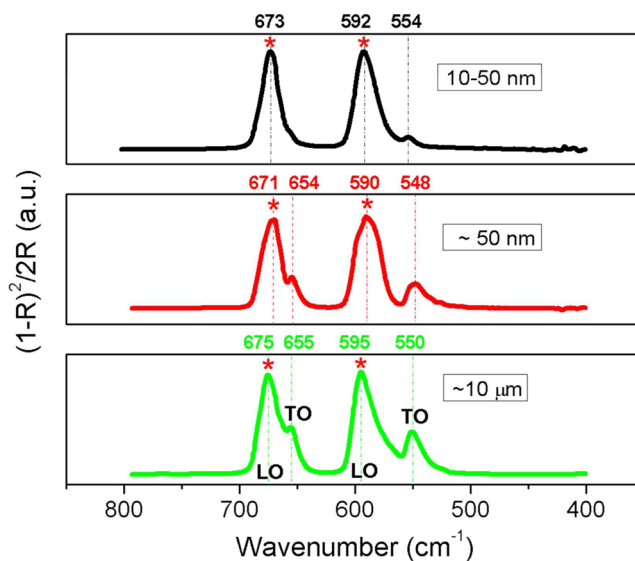


Figure 2. Diffuse reflectance of FTIR spectra of Co_3O_4 with three different average sizes: $\sim 10\text{ }\mu\text{m}$, $\sim 50\text{ nm}$, and $10\text{--}50\text{ nm}$. The $10\text{--}50\text{ nm}$ sample is obtained from $10\text{ }\mu\text{m}$ powders via ball milling.

particle sizes. Like transmission with a large incident angle above, all four phonons can be observed, but LO phonons appear stronger than TO modes, and the LO/TO intensity ratio increases when the average particle size decreases. Again, no noticeable change in the phonon peak position and line width is observed. The reason for the appearance of LO modes in diffuse reflectance spectra is that DRFTIR involves multiple reflections and transmissions through the Co_3O_4 particles at

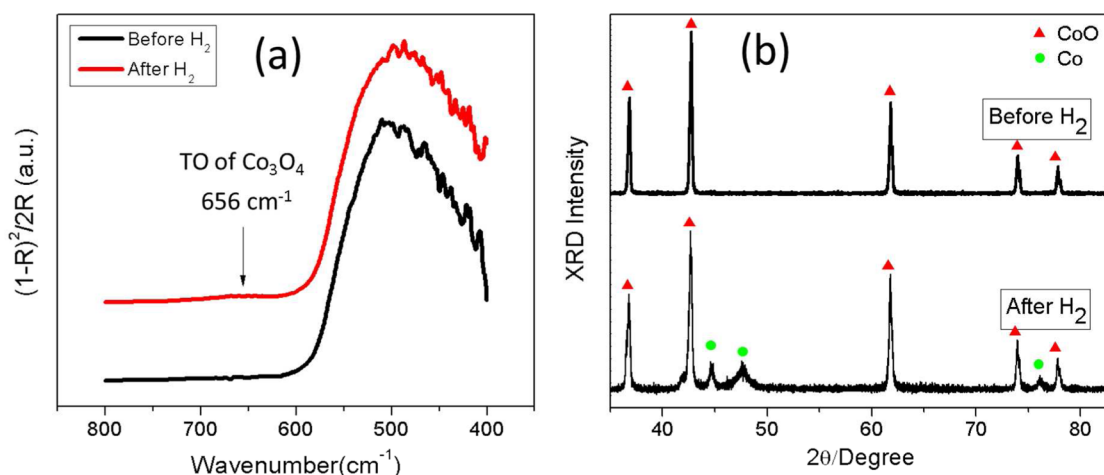


Figure 3. (a) Diffuse reflectance FTIR and (b) XRD spectra of CoO powders before and after H₂ treatment.

mostly oblique angles facilitated also by the KCl filler. As the particle size in the powder decreases, the normal reflecting particle surface diminishes as well due to the increase surface curvature. This, along with the increased scattering at large angles, results in the enhanced LO to TO intensity ratio.

3.3. LO Spectrum of CoO by Diffuse Reflectance.

DRFTIR was also employed to measure the LO spectrum of CoO powders. The TO phonon of CoO cannot be accessed by our system due to the limit of beam splitter and detector. Figure 3a shows the spectra of CoO obtained from 10 μm Co₃O₄ powders and similar spectra were also observed in CoO decomposed from 50 nm Co₃O₄ nanoparticles. On the basis of DRFTIR of Co₃O₄ and a previous study, the broad peak centered at 510 cm⁻¹ is assigned to the LO of CoO, which is very close to the spectrum reported by Tang et al.¹¹ A weak peak of Co₃O₄ phonon at ~656 cm⁻¹ can also be seen in Figure 3a in CoO without H₂ treatment. Figure 3b shows the corresponding XRD spectra; no Co₃O₄ can be observed, indicating that DRFTIR is a more sensitive technique than XRD. A side effect of annealing in H₂ is that a small amount of metallic Co was also produced, as revealed by XRD.

3.4. Spectral Conversion between CoO and Co₃O₄.

To further confirm the phonon spectrum of CoO and its relationship with that of Co₃O₄, we gradually oxidized CoO powders by heating in air on a hot plate and monitored the evolution of the spectrum. Figure 4a shows the DRFTIR spectrum after CoO was heat treated for 2 h at 300, 500, and 800 °C. It is well-known that CoO will transform to Co₃O₄ when oxidized in air. This transformation can be clearly seen; phonons of Co₃O₄ grow and the broad absorption feature of CoO begins to decrease when the temperature increases. This structural transition is also captured by XRD in Figure 4b, except that no Co₃O₄ was detected at 300 °C although two TO bands of Co₃O₄ are very visible, which further confirms that FTIR is a more sensitive technique than XRD. An interesting observation is that unlike DRFTIR of Co₃O₄ powders, TO is much stronger than LO at the early oxidation stages. This is because Co₃O₄ starts from a thin shell on CoO core due to the oxidation CoO particles in air. For a thin shell or film, TO is the dominant feature of the spectrum, similar to the transmission spectra shown in Figure 1.

The FTIR spectra can also be used to monitor the reverse process, that is, the decomposition of Co₃O₄ to CoO, during which oxygen will be released. Figure 5a shows the change in

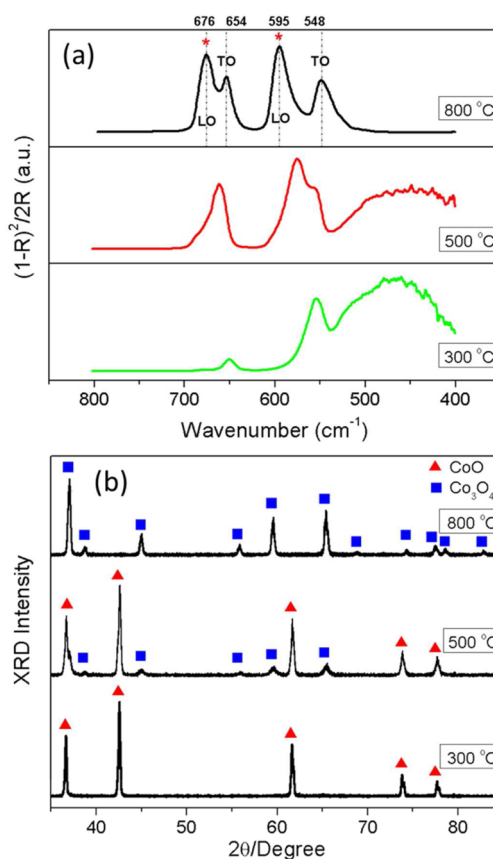


Figure 4. Oxidation of CoO to Co₃O₄. (a) Diffuse reflectance FTIR and (b) XRD spectra of CoO powders after heat treatment at 300, 500, and 800 °C for 2 h in air.

O₂ concentration when 10 μm Co₃O₄ powders were annealed in an Ar atmosphere (225 sccm) from 350 to 950 °C at a heating rate of 20 °C per minute. It can be seen that the decomposition started at ~700 °C and ended at ~870 °C, similar to previous observations.¹¹ On the basis of the oxygen release information, we annealed the Co₃O₄ powders at 700 °C for 60 min, 850 °C for 90 min, and 950 °C for 180 min; the annealed samples were denoted as Co-700, Co-850, and Co-950, respectively. The corresponding XRD patterns and FTIR spectra in Figure 5b,c confirm the transition from Co₃O₄ to CoO. Unlike the oxidation of CoO, the thermal decomposition

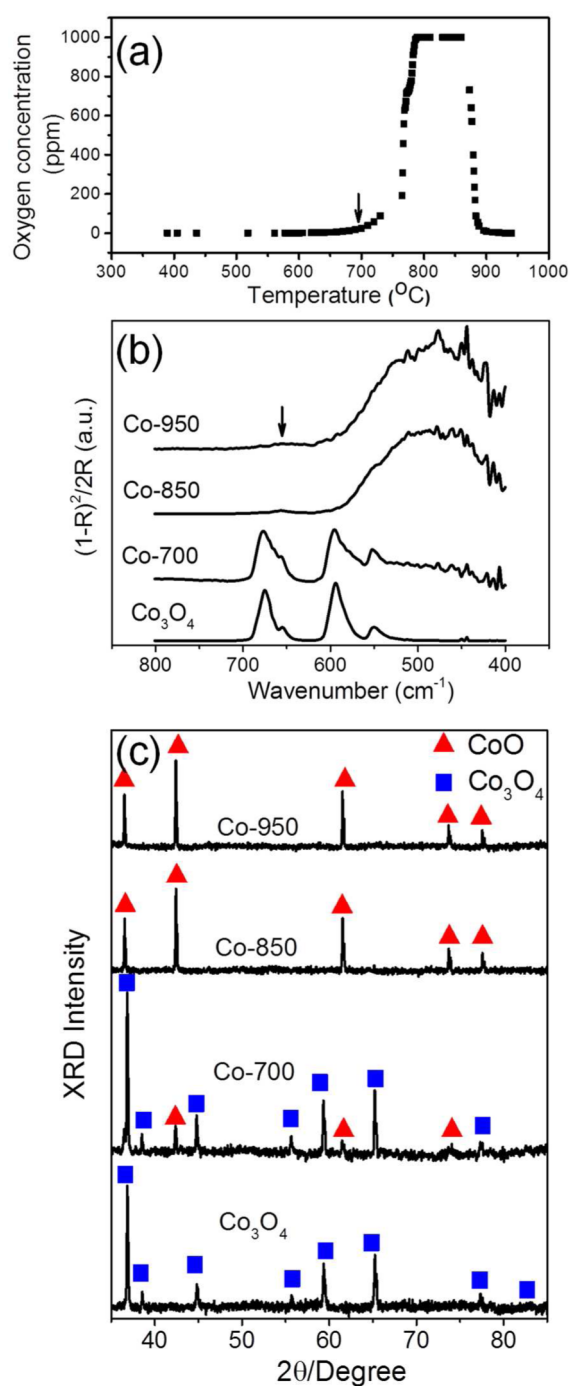


Figure 5. Thermal decomposition of Co_3O_4 to CoO . (a) Oxygen level in the annealing tube when the temperature increased from 350 to 950 °C at a rate of 20 °C per minute. (b) Diffuse reflectance FTIR and (c) XRD spectra of Co_3O_4 powders after heat treatment at 700, 850, and 950 °C in Ar.

of Co_3O_4 requires a higher temperature, indicating that Co_3O_4 is more stable in air than CoO .

3.5. Raman Spectrum of CoO . In defect-free CoO single crystals, the first-order phonon Raman scattering is forbidden according to the selection rules for the NaCl-type centrosymmetric lattice structure. In fact, as discussed above, CoO has three branches of optic phonons: two degenerate TO modes and one LO mode.³⁶ They are infrared active and cannot be Raman active in crystal lattice with center inversion symmetry.

The second-order two-phonon Raman scattering, however, is allowed, and accounting for the phonon dispersion of CoO ,^{36,37} it should appear in the 1000–1100 cm^{-1} spectral range.

Figure 6 shows the Raman spectra of H_2 annealed CoO film on Co foil measured in vacuum and at three different

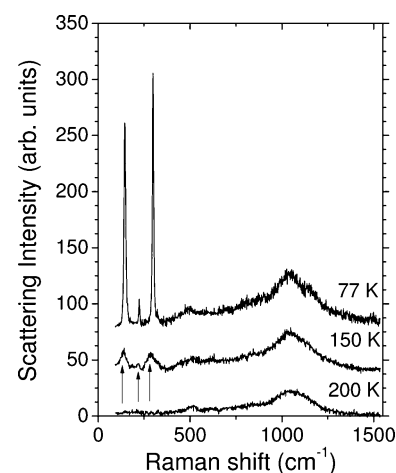


Figure 6. Raman Spectra of CoO excited with a 514 nm laser line at different temperatures.

temperatures with the 514 nm laser excitation at very low power. The room-temperature Raman spectrum of CoO is essentially the same as the bottom spectrum in Figure 6. The Raman spectra of pure CoO above 200 K, in which CoO is in paramagnetic state, are dominated by a broad band at $\sim 1060 \text{ cm}^{-1}$, which is consistent with the expected second-order Raman scattering from optical modes in CoO .³⁶ Similar band has also been reported by Struzhkin et al.³⁸ In addition, a weak band at 500–550 cm^{-1} is seen with varying spot-to-spot intensity. On the basis of the results of the lattice dynamics calculations,^{36,37} we assign this band to the defect-induced one-phonon density of states scattering in CoO . With decreasing temperature below 200 K, three new sharp peaks start to grow. They represent the Raman scattering from magnons in the antiferromagnetic CoO .^{38,39} At this point, we suggest that the ultimate Raman test for confirming the presence of CoO in a cobalt oxide mixture is the measurement of the magnon lines at low temperatures.

In the same study, Struzhkin et al. also observed a sharp peak at 697 cm^{-1} and assigned it to two-phonon Raman of CoO .³⁸ To investigate the origin of this line, we performed measurement at room temperature in another pure CoO sample. Figure 7 shows the Raman spectrum of CoO before and after the illumination of larger laser power (70 mW) for 2 min. This sharp line was observed only after laser heating, indicating that this line originates from Co_3O_4 due to partial oxidation of CoO by local laser heating. Figure 7a also shows the difference in Raman with two laser lines. A spectral shift of Raman band can be observed when the excitation energy is changed, a characteristic of two-phonon Raman.

3.6. More Discussion. We believe the reason why only two peaks were observed in previous FTIR studies of Co_3O_4 is because transmission with normal incidence was used.^{11,22,25–33} The reported high-frequency TO band of Co_3O_4 has a similar frequency as what we have observed around 660 cm^{-1} but the low-frequency TO band is 15–30 cm^{-1} higher than our observation of $\sim 555 \text{ cm}^{-1}$.^{11,22,25–33} On the basis of our

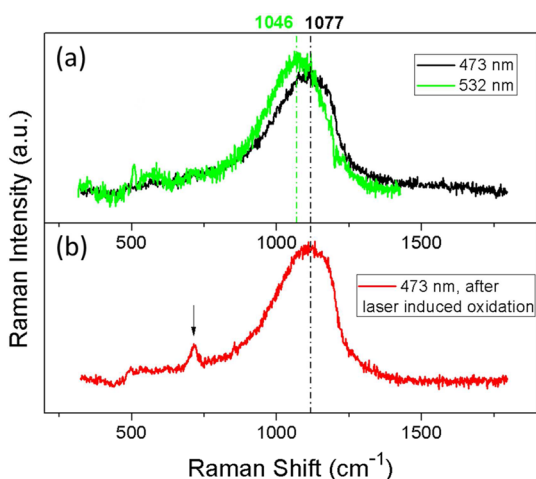


Figure 7. (a) Raman spectra of CoO excited with 473 and 532 nm laser lines. (b) Raman spectra of CoO excited with 20 mW 473 nm after exposure to 70 mW 473 nm laser beam.

consistent observation of this TO in thin films and powders, as well as previous studies by Shirai et al.²⁴ and Lenglet et al.,²¹ we believe that $\sim 555\text{ cm}^{-1}$ is a more accurate value of CoO TO. For Raman of CoO, many observed lines in the range of $450\text{--}700\text{ cm}^{-1}$ could come from partially oxidized CoO, or structural defects and impurities of CoO.^{11–17} Our observed CoO LO frequency of 510 cm^{-1} is at least 50 cm^{-1} lower than those obtained from reflectance measurement of single crystals or thin films,^{20–22} but this value agrees well with ab initio calculation³⁶ and two-phonon Raman of $\sim 1060\text{ cm}^{-1}$.³⁸ Note that according to phonon dispersion curve,³⁶ the phonon with the highest frequency is not located on the Brillouin zone edges, and it is $\sim 30\text{ cm}^{-1}$ higher than LO. The two-phonon joint density of states will become the largest around this phonon based on the dispersion curve.³⁶ In other words, the peak of two-phonon Raman should be larger than twice that of LO by $\sim 60\text{ cm}^{-1}$; clearly, a LO frequency of more than 560 cm^{-1} is too high to be in agreement with $\sim 1060\text{ cm}^{-1}$ two-phonon Raman. The weak but visible TO phonon at 656 cm^{-1} in untreated CoO in Figure 3 and in slightly oxidized CoO at $300\text{ }^\circ\text{C}$ in Figure 4 comes from Co_3O_4 .

4. CONCLUSIONS

In summary, we have demonstrated that all four phonons above 500 cm^{-1} can be observed in thin films and powders of Co_3O_4 . The low (high)-frequency TO is located at 552 ± 4 (655 ± 1) cm^{-1} with LO-TO splitting of 43 ± 4 (21 ± 4) cm^{-1} . CoO powders can be identified by a broad IR band around 510 cm^{-1} ; Raman spectrum of CoO is represented by a two-phonon peak at $\sim 1060\text{ cm}^{-1}$ at room temperature as well as magnon lines below 300 cm^{-1} at low temperature. The LO and two-phonon Raman band of CoO agree well with theoretical calculations. For thin films, a large oblique incident angle is required to observe both TO and LO phonons, but for particle or powder samples diffuse reflectance is a convenient, effective, and safe method. Intensity of laser excitation should be kept low in CoO Raman scattering in order to avoid thermal oxidation of CoO. Our optical spectroscopic techniques and self-consistent spectra will accelerate the progress in basic understanding and future applications of cobalt oxides.

AUTHOR INFORMATION

Corresponding Author

*E-mail: jbao@uh.edu.

Notes

The authors declare no competing financial interest.

ACKNOWLEDGMENTS

Jiming Bao acknowledges support from the Robert A Welch Foundation (E-1728) and the National Science Foundation (Career Award ECCS-1240510).

REFERENCES

- (1) Li, Y.; Tan, B.; Wu, Y. Mesoporous Co_3O_4 Nanowire Arrays for Lithium Ion Batteries with High Capacity and Rate Capability. *Nano Lett.* **2008**, *8*, 265–270.
- (2) Makhlof, S. A. Magnetic Properties of Co_3O_4 Nanoparticles. *J. Magn. Magn. Mater.* **2002**, *246*, 184–190.
- (3) Yamaura, H.; Moriya, K.; Miura, N.; Yamazoe, N. Mechanism of Sensitivity Promotion in Co Sensor Using Indium Oxide and Cobalt Oxide. *Sens. Actuators, B* **2000**, *65*, 39–41.
- (4) Amatucci, G. G.; Tarascon, J. M.; Klein, L. C. CoO_2 , the End Member of the Li_xCoO_2 Solid Solution. *J. Electrochem. Soc.* **1996**, *143*, 1114–1123.
- (5) Reimers, J. N.; Dahn, J. R. Electrochemical and in-Situ X-Ray-Diffraction Studies of Lithium Intercalation in Li_xCoO_2 . *J. Electrochem. Soc.* **1992**, *139*, 2091–2097.
- (6) Zhang, N.; Shi, J. W.; Mao, S. S.; Guo, L. J. Co_3O_4 Quantum Dots: Reverse Micelle Synthesis and Visible-Light-Driven Photocatalytic Overall Water Splitting. *Chem. Commun.* **2014**, *50*, 2002–2004.
- (7) Ma, C. Y.; Mu, Z.; Li, J. J.; Jin, Y. G.; Cheng, J.; Lu, G. Q.; Hao, Z. P.; Qiao, S. Z. Mesoporous Co_3O_4 and Au/ Co_3O_4 Catalysts for Low-Temperature Oxidation of Trace Ethylene. *J. Am. Chem. Soc.* **2010**, *132*, 2608–2613.
- (8) Minnermann, M.; Grossmann, H. K.; Pokhrel, S.; Thiel, K.; Hagelin-Weaver, H.; Baumer, M.; Madler, L. Double Flame Spray Pyrolysis as a Novel Technique to Synthesize Alumina-Supported Cobalt Fischer–Tropsch Catalysts. *Catal. Today* **2013**, *214*, 90–99.
- (9) Polisetty, S.; Echtenkamp, W.; Jones, K.; He, X.; Sahoo, S.; Binek, C. Piezoelectric Tuning of Exchange Bias in a $\text{BaTiO}_3/\text{Co}/\text{CoO}$ Heterostructure. *Phys. Rev. B: Condens. Matter Mater. Phys.* **2010**, *82*, 134419–134425.
- (10) Liao, L.; et al. Efficient Solar Water Splitting Using a Nanocrystalline CoO Photocatalyst. *Nat. Nanotechnol.* **2014**, *9*, 69–73.
- (11) Tang, C. W.; Wang, C. B.; Chien, S. H. Characterization of Cobalt Oxides Studied by FT-IR, Raman, TPR and TG-MS. *Thermochim. Acta* **2008**, *473*, 68–73.
- (12) Wang, W. Z.; Zhang, G. L. Synthesis and Optical Properties of High-Purity CoO Nanowires Prepared by an Environmentally Friendly Molten Salt Route. *J. Cryst. Growth* **2009**, *311*, 4275–4280.
- (13) Gallant, D.; Pezolet, M.; Simard, S. Optical and Physical Properties of Cobalt Oxide Films Electrogenerated in Bicarbonate Aqueous Media. *J. Phys. Chem. B* **2006**, *110*, 6871–6880.
- (14) Vuurman, M. A.; Stufkens, D. J.; Oskam, A.; Deo, G.; Wachs, I. E. Combined Raman and IR Study of $\text{MO}_x\text{-V}_2\text{O}_5/\text{Al}_2\text{O}_3$ ($\text{MO}_x = \text{MoO}_3, \text{WO}_3, \text{NiO}, \text{CoO}$) Catalysts under Dehydrated Conditions. *J. Chem. Soc., Faraday Trans.* **1996**, *92*, 3259–3265.
- (15) Melendres, C. A.; Xu, S. In Situ Laser Raman Spectroscopic Study of Anodic Corrosion Films on Nickel and Cobalt. *J. Electrochem. Soc.* **1984**, *131*, 2239–2243.
- (16) Ravindra, A. V.; Behera, B. C.; Padhan, P. Laser Induced Structural Phase Transformation of Cobalt Oxides Nanostructures. *J. Nanosci. Nanotechnol.* **2014**, *14*, 5591–5595.
- (17) Choi, H. C.; Jung, Y. M.; Noda, I.; Kim, S. B. A Study of the Mechanism of the Electrochemical Reaction of Lithium with CoO by Two-Dimensional Soft X-Ray Absorption Spectroscopy (2D XAS), 2D

Raman, and 2D Heterospectral XAS-Raman Correlation Analysis. *J. Phys. Chem. B* **2003**, *107*, 5806–5811.

(18) Struzhkin, V. V.; Goncharov, A. F.; Syassen, K. Effect of Pressure on Magnetic Excitations in CoO. *Mater. Sci. Eng., A* **1993**, *168*, 107–110.

(19) Barakat, N. A. M.; Khil, M. S.; Sheikh, F. A.; Kim, H. Y. Synthesis and Optical Properties of Two Cobalt Oxides (CoO and Co₃O₄) Nanofibers Produced by Electrospinning Process. *J. Phys. Chem. C* **2008**, *112*, 12225–12233.

(20) Kant, C.; Rudolf, T.; Schrettle, F.; Mayr, F.; Deisenhofer, J.; Lunkenheimer, P.; Eremin, M. V.; Loidl, A. Optical Spectroscopy in CoO: Phononic, Electric, and Magnetic Excitation Spectrum within the Charge-Transfer Gap. *Phys. Rev. B: Condens. Matter Mater. Phys.* **2008**, *78*, 245103–245113.

(21) Lenglet, M.; Lopitiaux, J.; Terrier, L.; Chartier, P.; Koenig, J. F.; Nkeng, E.; Poillerat, G. Initial Stages of Cobalt Oxidation by FTIR Spectroscopy. *J. Phys. IV* **1993**, *3*, 477–483.

(22) Pfeil, T. L.; Pourpoint, T. L.; Groven, L. J. Effects of Crystallinity and Morphology of Solution Combustion Synthesized Co₃O₄ as a Catalyst Precursor in Hydrolysis of Sodium Borohydride. *Int. J. Hydrogen Energy* **2014**, *39*, 2149–2159.

(23) Hadjiev, V. G.; Iliev, M. N.; Vergilov, I. V. The Raman Spectra of Co₃O₄. *J. Phys. C: Solid State Phys.* **1988**, *21*, 199–201.

(24) Shirai, H.; Morioka, Y.; Nakagawa, I. Infrared and Raman Spectra and Lattice Vibrations of Some Oxide Spinel. *J. Phys. Soc. Jpn.* **1982**, *51*, 592–597.

(25) Pejova, B.; Isahi, A.; Najdoski, M.; Grozdanov, I. Fabrication and Characterization of Nanocrystalline Cobalt Oxide Thin Films. *Mater. Res. Bull.* **2001**, *36*, 161–170.

(26) Varghese, S.; Cutrufello, M. G.; Rombi, E.; Monaci, R.; Cannas, C.; Ferino, I. Mesoporous Hard-Templated Me-Co [Me = Cu, Fe] Spinel Oxides for Water Gas Shift Reaction. *J. Porous Mater.* **2014**, *21*, 539–549.

(27) Salavati-Niasari, M.; Mir, N.; Davar, F. Synthesis and Characterization of Co₃O₄ Nanorods by Thermal Decomposition of Cobalt Oxalate. *J. Phys. Chem. Solids* **2009**, *70*, 847–852.

(28) Farhadi, S.; Safabakhsh, J.; Zaringhadam, P. Synthesis, Characterization, and Investigation of Optical and Magnetic Properties of Cobalt Oxide (Co₃O₄) Nanoparticles. *Journal of Nanostructure in Chemistry* **2013**, *3*, 69–77.

(29) Kelpsaite, I.; Baltrusaitis, J.; Valatka, E. Electrochemical Deposition of Porous Cobalt Oxide Films on AISI 304 Type Steel. *Materials Science* **2011**, *17*, 236–243.

(30) Liu, Y.; Zhu, G.; Ge, B.; Zhou, H.; Yuan, A.; Shen, X. Concave Co₃O₄ Octahedral Mesocrystal: Polymer-Mediated Synthesis and Sensing Properties. *CrystEngComm* **2012**, *14*, 6264–6270.

(31) Yue, W.; Lin, Z.; Jiang, S.; Yang, X. Preparation of Graphene-Encapsulated Mesoporous Metal Oxides and Their Application as Anode Materials for Lithium-Ion Batteries. *J. Mater. Chem.* **2012**, *22*, 16318–16323.

(32) Athar, T.; Hakeem, A.; Topnani, N.; Hashmi, A. Wet Synthesis of Monodisperse Cobalt Oxide Nanoparticles. *ISRN Materials Science* **2012**, *2012*, 1–5.

(33) Bhatt, A. S.; Bhat, D. K.; Tai, C.-w.; Santosh, M. S. Microwave-Assisted Synthesis and Magnetic Studies of Cobalt Oxide Nanoparticles. *Mater. Chem. Phys.* **2011**, *125*, 347–350.

(34) Khodakov, A. Y.; Lynch, J.; Bazin, D.; Rebours, B.; Zanier, N.; Moisson, B.; Chaumette, P. Reducibility of Cobalt Species in Silica-Supported Fischer–Tropsch Catalysts. *J. Catal.* **1997**, *168*, 16–25.

(35) Berreman, D. Infrared Absorption at Longitudinal Optic Frequency in Cubic Crystal Films. *Phys. Rev.* **1963**, *130*, 2193–2198.

(36) Wdowik, U. D.; Parlinski, K. Lattice Dynamics of CoO from First Principles. *Phys. Rev. B: Condens. Matter Mater. Phys.* **2007**, *75*, 104306–104311.

(37) Wdowik, U. D.; Parlinski, K. Lattice Dynamics of Cobalt-Deficient CoO from First Principles. *Phys. Rev. B: Condens. Matter Mater. Phys.* **2008**, *78*, 224114–224121.

(38) Struzhkin, V. V.; Goncharov, A. F.; Syassen, K. Effect of Pressure on Magnetic Excitations in CoO. *Mater. Sci. Eng., A* **1993**, *168*, 107–110.

(39) Hayes, R. R.; Perry, C. H. Magnetic Excitations in Cobalt Oxide. *Solid State Commun.* **1974**, *14*, 173–175.